Article

A Novel Direct Optimization Framework for Hypersonic Waverider Inverse Design Methods

Jiwon Son [1] , Chankyu Son [2] and Kwanjung Yee [1,*]

1   Department of Aerospace Engineering, Seoul National University, Seoul 08826, Korea; forscing@gmail.com
2   Department of Unmanned Aircraft Systems, Cheongju University, Cheongju 28503, Korea; cson@cju.ac.kr
*   Correspondence: kjyee@snu.ac.kr; Tel.: +82-2-880-4151

Abstract: Waverider is a hypersonic vehicle that improves the lift-to-drag ratio using the shockwave attached to the leading edge of the lifting surface. Owing to its superior aerodynamic performance, it exhibits a viable external configuration in hypersonic flight conditions. Most of the existing studies on waverider employ the inverse design method to generate vehicle configuration. However, the waverider inverse design method exhibits two limitations; inaccurate definition of design space and unfeasible performance estimation during the design process. To address these issues, a novel framework to directly optimize the waverider is proposed in this paper. The osculating cone theory is adopted as a waverider inverse design method. A general methodology to define the design space is suggested by analyzing the design curves of the osculating cone theory. The performance of the waverider is estimated accurately and rapidly via combining a high-fidelity computational fluid dynamics solver and a surrogate model. A comparison study shows that the proposed direct optimization framework enables a more accurate design space and efficient performance estimation. The framework is applied to the multi-objective optimization problem, which maximizes internal volume and minimizes aerodynamic drag. Finally, general characteristics for waverider are presented by analyzing the optimized results with data mining methods such as K-means.

Keywords: waverider; hypersonic vehicle; osculating cone theory; inverse design; optimization

1. Introduction

Hypersonic vehicles, which have the advantage of prompt global reach, are being actively researched as next-generation transport systems worldwide, especially in the United States and China [1]. In a hypersonic environment, the vehicle experiences extreme aerodynamic heating, dynamic instability, and a decrease in the lift-to-drag ratio (L/D) due to the wave drag [2]. This decrease is a major factor that reduces the cruising efficiency of the vehicle in terms of range and endurance. Since a hypersonic vehicle spends most of its flight time in a cruising state, the overall performance may be critically reduced by its low L/D. Therefore, it is essential to investigate the external configuration of the hypersonic vehicle that significantly affects the L/D.

A waverider with a high L/D under the hypersonic condition was developed by Nonweiler as a hypersonic vehicle concept in 1959 [3]. The waverider is a supersonic lifting body characterized by an attached bow shockwave along its leading edge [4], which eliminates the flow spillage from the lower surface to the upper surface. Consequently, high pressure generated by the shockwave affects only the lower surface of the vehicle. Therefore, the waverider exhibits a higher L/D than other lifting bodies. Owing to its superior aerodynamic performance, the waverider is regarded as the best among hypersonic aircraft.

Along with the new hypersonic vehicle concept, the waverider suggested by Nonweiler [3] introduced a design methodology to generate the waverider configuration. Herein, the shape of the shockwave is determined by the vehicle configuration and flow conditions. Therefore, to identify a vehicle configuration with an attached shockwave

along the leading edge, it is necessary to repeat the process of fabricating the shape of the aircraft and verifying whether the generated shockwave is attached to the leading edge. To address this issue, Nonweiler suggested the inverse design method for the waverider, which comprises the following three steps:

(1)　Generating the basic flow field

In addition, the first step in designing a waverider is to generate a flow field that occurs around a vehicle before deciding the waverider configuration. The flow properties, including the shape of the shockwave, are determined in this step;

(2)　Defining the leading edge

In the second step, the leading-edge shape is defined to derive the waverider configuration. Since the shockwave must be attached along the leading edge of the vehicle, the shape of the leading edge is drawn on the shockwave plane. Additionally, the surface generated by moving the leading-edge shape parallel to the freestream direction is determined as the upper surface of the vehicle. This ensures that the shockwave is not generated on the upper surface;

(3)　Deriving the waverider configuration using the streamline tracing technique

In the final stage of the design, the lower surface of the vehicle is defined. Initially, the leading edge is discretized. Considering that each discretized point is within the basic flow field defined in step (1), the streamline is traced for each point. As the streamline must be parallel to the wall because of the supersonic boundary condition, a shockwave identical to that of the basic flow field is generated when these streamlines are combined and used as the lower surface. Therefore, streamlines compose the lower surface of the waverider. The designing of the waverider is completed when the rear of the vehicle is defined to be perpendicular to the free flow.

The three-step inverse design method has been improved through several studies [5–8]. Jones developed a new waverider design method that improves volumetric efficiency by employing a conical flowfield as the basic flowfield to a conical flow field [5]. Rasmussen designed a waverider with the basic flowfield around the elliptic cone [6]. Sobieczky developed the osculating cone theory to enable waverider design even if the basic flowfield is not an actual flow field [7]. Osculating cone theory has paved the way for waverider inverse design to have a higher degree of design freedom by greatly expanding the range of the shockwave shape. Subsequently, Chen extended the osculating cone theory and presented a methodology that can be designed for variable shock angles, and Zheng presented a design methodology that can define the shape of the shockwave surface in three dimensions [8,9]. With these research achievements, the inverse design method became the standard for waverider design.

Nevertheless, the inverse design method exhibits two inherent problems [10,11], namely the design space and performance estimation. The inverse design method begins with the resultant physical phenomena, such as the shape of the shockwave. Thus, the design method cannot derive the solution if an impractical shockwave shape is defined. Therefore, the design space is defined by establishing whether the shape of the shockwave is realistic. Since it is difficult to determine the reality in advance, the definition of the design space is highly complicated.

Furthermore, the performance of the designed waverider is not directly estimated with the inverse design method. For instance, in the case of a waverider, vehicle configuration satisfies the design requirement of a leading edge attached shockwave. However, the performance of the vehicle, such as lift or drag, is not estimated. Consequently, the inverse design method cannot be employed directly on the optimization as design objectives and constraints cannot be imposed.

The aforementioned problems result in certain limitations, such as using only a part of the design freedom and incorrectly predicted performance, in the waverider design. Moreover, the combination of the two problems prevents optimization, which restricts the waverider from exhibiting its optimal performance.

To address the design space and performance estimation problems of the inverse design method, direct optimization of the waverider was suggested by Takashima [12], wherein the osculating cone theory, developed by Sobieczky [7], was used to generate the waverider configuration. For the design space problem, Takashima suggested an osculating cone theory-based design space equation formulated by determining design variables empirically, which generate an unrealistic shockwave shape. The performance estimation problem was addressed by predicting the aerodynamic forces acting on the vehicle using the tangent-cone method, which is a type of surface inclination method. After addressing the two problems of the inverse design method, Takashima performed optimization to identify the best performing waverider configuration. Thus, an optimal design of the waverider that maximizes the L/D was obtained. However, the empirically obtained design space equation is valid only for the limited design parameters used by Takashima. Thus, designers must determine a new design space with each change in the design conditions, such as the range of design variables and the shape of design parameters. Moreover, using the tangent-cone method to predict the high-pressure flow characteristics that occur in large, curved shapes is challenging.

Considering the design space problem, Kontogiannis et al. [13] suggested parametric waverider geometry models for the osculating cone theory, which can be applied to waveriders with a higher degree of freedom (DOF). The investigations reported that the design space of the waverider is constrained by the vertical position of the leading edge, and the inverse design cannot be executed if the position of the leading edge is extremely low. Although Kontogiannis et al. considered the effect of the leading edge on the design space, the effect of the shape of the shockwave was excluded. As unrealistic shockwave shapes can also cause design space problems, the shape of the shockwave needs to be investigated to define an accurate design space.

Furthermore, Lobbia [14,15] developed an aerodynamics analysis tool to evaluate the performance of the vehicle by calculating the aerodynamic forces acting on a vehicle with high fidelity through the integration of modified Newtonian, tangent-cone, and shock/expansion methods. Although the aerodynamic force was calculated accurately unlike previous studies, the calculation time was not reduced and the design required numerous computational resources.

In summary, the design space and performance estimation problems of the inverse design method can be addressed by the direct optimization approach. Although efforts have been made to improve this approach, such as the performance estimating technique of Lobbia and design space analysis of Kontogiannis, they have certain limitations.

Therefore, we propose a new direct optimization framework for a waverider inverse design. The direct optimization framework consists of two modules that deal with the issues of inverse design and waverider configuration generating module. To address the design space problem, a general methodology that can derive a design space for a waverider based on the osculating cone theory was proposed. We used a discriminant formula to determine whether the design parameter is realistic. The simultaneous consideration of the effect of the leading edge and shockwave generated a more accurate design space equation. Furthermore, the performance estimation problem is addressed using a high-fidelity flow analysis solver based on the Euler equation that can calculate the aerodynamic forces acting on a waverider. Additionally, a surrogate model evaluated the performance of the designed waverider to decrease the required number of computational resources. The direct optimization framework was completed by applying the above processes to the modules. Finally, we performed optimization to identify the best performing waverider configuration. The Pareto design solutions obtained by the completed design process achieved a high internal volume with low drag. Moreover, the significant factors influencing the waverider performance and general characteristics of configuration were identified using data mining methods, such as K-means clustering, analysis of variance (ANOVA) and decision tree analysis.

2. Methodology

To overcome the two limitations of the waverider inverse design, a design space-defining methodology and performance estimation technique are presented in this paper. Section 2 presents a generalized application process of the direct design framework, wherein a design space-defining methodology and performance estimation technique are applied. Section 2.1 describes the implementation process of the direct design framework. The theory and validation for establishing the design space-defining methodology are described in Section 2.2. The detailed methods used in the performance estimation technique are explained in Section 2.3.

2.1. Direct Design Approach

Figure 1 illustrates the three modules in the direct optimization framework for the waverider, namely the: (1) problem definition; (2) waverider inverse design; and (3) model construction. The design space for the waverider is defined in the problem definition module. The model construction module evaluates the performance of the waverider and generates a surrogate model with the performance estimation technique. Waverider configuration is generated in the waverider inverse design module. The osculating cone theory, which can ensure a high design DOF, was employed in this study. The details of the osculating cone theory are described in the Appendix A.
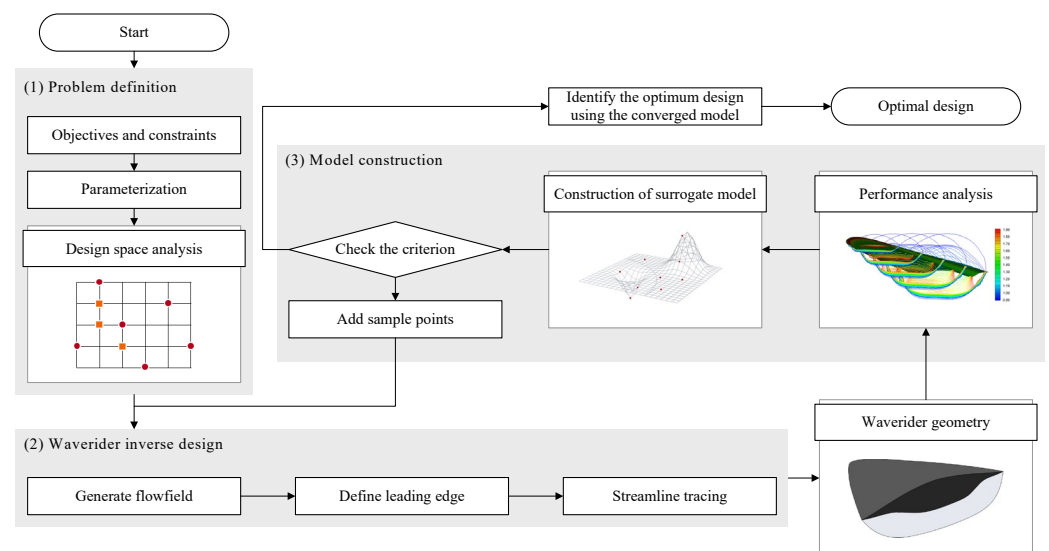

Figure 1. Direct optimization framework for waverider.

The direct design approach begins with the problem definition module. Initially, the design objectives and constraints are formulated in terms of performance variables to reflect the purpose of the design. Subsequently, design parameters for the waverider are defined by representing the shape of the shockwave and the waverider with design curves, such as Bezier curves. Finally, the design space is derived using the proposed design space-defining methodology, which involves deriving the discriminant formula by analyzing the osculating cone theory and applying the discriminant formula to the design parameters. The lattice space expressed in the problem definition module of Figure 1 represents the design space.

The model construction module begins after deriving the waverider configurations. Computational fluid dynamics (CFD) is used to calculate the performance (such as the lift and drag) of the waverider. However, as CFD analysis requires extensive computational resources, it cannot be used directly in the design process owing to the numerous estimations. To address this problem, a surrogate model is employed to represent the performance of the waverider. This surrogate model enables fast computation by expressing the relationship between the result of the CFD and the design parameters as a numerical formula. The

generation of the surrogate model requires design parameters and a performance estimation dataset. The design of experiment (DOE) is performed to select the dataset efficiently. Initially, the design parameters are selected, as represented by circles in the design space (Figure 1). After selecting the design parameters, the waverider configuration of each parameter is generated in the waverider inverse design module. Subsequently, the performance of each configuration is estimated using the CFD analysis. The surrogate model is constructed with the datasets that comprise these results and the design parameters. The accuracy of the constructed model is enhanced by data addition, which is iteratively conducted identically to the DOE. The model construction is terminated when the model surpasses a certain accuracy level after repeated addition. The squares in the design space (Figure 1) represent the added points.

The problem definition and model construction modules are followed by optimization. In this study, a genetic algorithm is used as the optimization method [16], which applies natural selection to optimize and robustly identify the non-linear maximum and minimum values of the model. A rank-based fitness assignment technique developed by Fonseca was used for selection in the genetic algorithm [17]. The fitness of each solution is estimated by calculating the number of dominated solutions in this method.

2.2. Design Space Defining Methodology

This section explains the design space-defining methodology. The design parameter of the inverse design is defined in terms of resultant physical phenomena, which is the shape of the shockwave in the case of waveriders. Therefore, the result cannot be obtained using the inverse design if an impractical design parameter is imposed. The design space of the inverse design is the feasible region obtained considering a practical design parameter. To derive this design space, we identified the design parameters that cause the failure of the inverse design. Subsequently, the design space was expressed in the form of a discriminant formula based on mathematical analysis, and the design space was compared with previously reported design spaces in the literature for performance verification.

Initially, the undesignable design parameters that limit the design space should be identified to derive the design space. The design parameters that cause the failure of the inverse design were expressed through geometric relationships based on design curves reported in the studies of Takashima and Kontogiannis [12,13]. The geometric relationships can be classified as: (a) the upper surface curve located above the center of the osculating cone, and (b) the osculating planes intersecting under the upper surface. Figure 2 illustrates the two constraints expressed using design curves on the osculating plane and base plane. Figure 2a depicts the relationship between the center of the local osculating cone and the upper surface of the waverider on the osculating plane. The solid line $P_1 - P_2 - P_3$ denotes a feasible design case, whereas the dashed line $P_4 - P_5$ indicates an infeasible design case. In the case of the feasible design, the upper surface curve $P_1 - P_2$ is below the center of the local osculating cone and the lower surface curve $P_2 - P_3$ is formed in a downward direction. Conversely, the upper surface curve $P_4 - P_5$ is located above the center of the local osculating cone in the case of the infeasible design. Herein, a streamline that begins from point P_5 is generated in an upward direction, and it cannot encompass the lower surface of the vehicle. Therefore, the upper surface curve must be located below the center of the osculating cone. Figure 2b depicts the osculating planes, upper surface curve, and shockwave curve on the base plane. The filled circle indicates the intersection point of the two osculating planes, wherein each osculating plane has its flow field. If the intersection point is below the upper surface curve, it exhibits the physical quantity of both osculating planes simultaneously. As two physical quantities cannot concurrently exist at one point, the waverider inverse design cannot derive the resultant configuration in this scenario. Therefore, the osculating planes must not intersect below the upper surface curve.
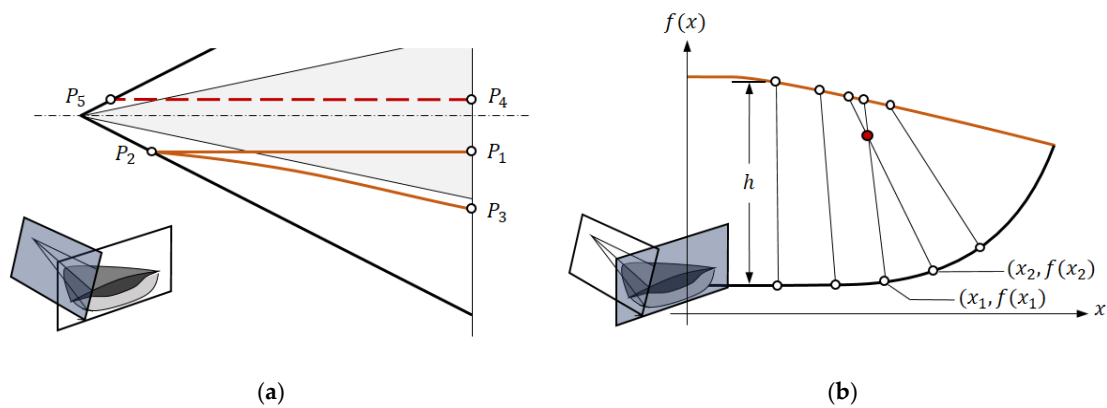
(a)　　　　　　　　　　　　　　**(b)**

Figure 2. Geometric relationships in the osculating cone theory: (**a**) Geometric constraint based on the position of the cone center; (**b**) Geometric constraint based on the intersected planes.

We analyzed the aforementioned two geometric relationships by representing the shockwave curve as a two-dimensional (2D) coordinate system on the base plane to derive the design space formula. As illustrated in Figure 2b, x denotes the spanwise distance between the center axis of the waverider and the discretized point of the shockwave. The vertical position of the discretized point of the shockwave is expressed as a function $f(x)$. The distance between the shockwave and the upper surface within the osculating plane is denoted as h. To avoid the first geometric relationship, the center of the local osculating cone must be above the upper surface. It can be expressed using Equation (1) considering the radius of curvature R.

$$R = \frac{\left[1 + \left(\frac{df}{dx}\right)^2\right]^{\frac{3}{2}}}{\frac{d^2 f}{dx^2}} > h. \tag{1}$$

For the second geometric relationship, the osculating planes must not intersect below the upper surface curve. We identified the intersection point of the two osculating planes by assuming that the planes coexist. Considering that each osculating plane does not intersect with the neighboring plane under the upper surface, all planes do not intersect under the upper surface. Further, we selected arbitrary neighboring osculating planes; their shockwave points were represented as x_1 and x_2. Finally, the coordinate x of the intersection point of the two osculating planes was derived, as presented in Equation (2).

$$\left(\frac{1}{\left[\frac{df}{dx}\right]_{x_2}} - \frac{1}{\left[\frac{df}{dx}\right]_{x_1}}\right) x = \left(\frac{x_2}{\left[\frac{df}{dx}\right]_{x_2}} - \frac{x_1}{\left[\frac{df}{dx}\right]_{x_1}}\right) + f(x_2) - f(x_1). \tag{2}$$

Equation (3) indicates the constraint formulated for the vertical coordinate of the intersection point to be above the upper surface. To satisfy this condition, x_2 was represented as $x_1 + dx$, and certain transformations were performed.

$$(x_1 - x) \frac{\left(1 + \left[\frac{df}{dx}\right]_{x_1}^2\right)^{\frac{1}{2}}}{\left[\frac{df}{dx}\right]_{x_1}} > h. \tag{3}$$

The left-hand side of Equation (3) is identical to that of Equation (1), which implies that the design space constraints described as geometric relationships are redundant. Therefore, the design constraints treated as separate in the literature must be unified. We used Equation (1) that unifies the entire design constraints as a "discriminant formula" for the osculating cone theory.

The design space can be formulated by applying the discriminant formula to each osculating plane. When Equation (1) is applied, the minimum radius of curvature of each osculating plane point is determined as a function of the shockwave. The most restrictive condition obtained by the discriminant formula represents the required design space.

We compared the design space-defining methodology with the design space constraint reported by Takashima [12]. The design curves and the design parameters defined by Takashima are depicted on the left-hand side of Figure 3. The upper surface curve was defined as a linear segment and a third-order Bezier curve, whereas the shockwave curve was defined as a linear segment and a fourth-order polynomial. Furthermore, x_{shock} and y_{shock} denote the width and height of the shockwave, respectively, and both variables are normalized to the entire length of the vehicle. Furthermore, x_{flat} indicates the length of the linear segment normalized to x_{shock}.
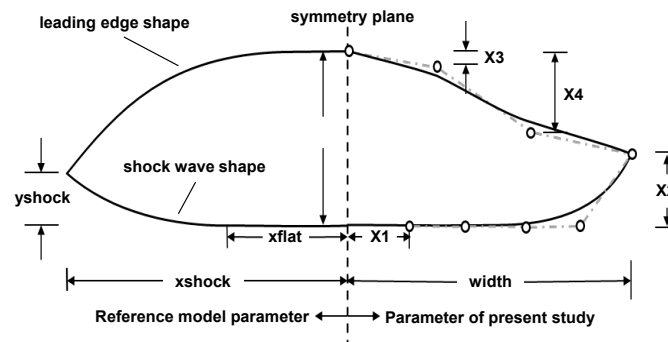

Figure 3. Waverider design curves and design parameters at the base plane.

In the study of Takashima, the design space of the waverider was constrained by defining the maximum value of y_{shock} as indicated in Equation (4). Here, $z_{waverider}$ denotes the normalized waverider length affecting the distance between the upper surface and the shockwave of the waverider. As x_{shock} increases or $z_{waverider}$ decreases, the feasible range of the y_{shock} between 0 and $y_{shock,max}$, which represents the design space, widens.

$$y_{shock,max} = 0.75(x_{shock} - 0.11) - 0.111(z_{waverider} - 0.31) + 0.0275. \tag{4}$$

In this study, we applied the discriminant formula [Equation (1)] to the design curves and design parameters reported by Takashima, which are illustrated in Figure 3, to derive the design space. As the linear segment of the shockwave has an infinite radius of curvature, the osculating planes that intersect the linear segment do not violate the constraint. In the case of the fourth-order polynomial region, the radius of curvature of each osculating plane point changes along the spanwise direction. Since it is difficult to compare the radius of curvature and the distance between the upper surface and shockwave before generating the waverider configuration, the lowest position of the local osculating cone among all osculating planes was identified and compared with the highest position of the upper surface. Consequently, the design space of this study was derived as presented in Equation (5), where β denotes the shockwave angle of the osculating cone. Equation (5) constrains the design space by limiting the maximum value of y_{shock}, similar to that in Equation (4). Additionally, the effect of x_{flat} was added to Equation (5).

$$y_{shock,max} = \frac{7}{64} \frac{x_{shock}^4 \left(1 - x_{flat}\right)^4}{z_{waverider}^3 \tan^3 \beta}. \tag{5}$$

The design spaces obtained from Equations (4) and (5) are depicted in Figure 4. To visualize the difference between the two design spaces, we plotted the isosurfaces for $y_{shock,max}$ at 0.01 and 0.07 based on the three variables, namely x_{shock}, x_{flat}, and $z_{waverider}$, in the three-dimensional (3D) space. The design space of Takashima is represented by

surfaces S_1 and S_3, and the region surrounded by surfaces S_2 and S_4 indicates that of the present study. The design space defined by Takashima cannot consider the variable x_{flat} [Equation (4)]. Therefore, a substantial difference exists between the design spaces reported by Takashima and in this study. The design space of this study expands as $z_{waverider}$ increases, whereas that reported by Takashima does not change. Figure 4a,b illustrate the cross-sections of the $z_{waverider}$ axis at 0.3 and 0.4, respectively. The filled circles denote the design points that cause the failure of the inverse design, and the empty circles represent the feasible design points. In Figure 4a, the values of y_{shock} of the design points indicated by empty circles are 0.001, 0.02, and 0.06; in Figure 4b, they are 0.005, 0.01, 0.04, and 0.06. Although the points with y_{shock} values of 0.001 and 0.005 are not included between the points with values of 0.01 to 0.07, the points are included in the design space because the design space is defined considering the maximum value for y_{shock}. Figure 4a depicts a design space reported by Takashima that does not overlap with the design space of this study. A design point included in this design space causes the failure of the design. Therefore, this design space must be excluded. Figure 4b illustrates the design point that can be designed despite it not belonging to the design space of Takashima. This design point must be included in the design space. In summary, Figure 4a,b verify that the design space derived in this study is more accurate than that reported by Takashima. Therefore, the proposed design space-defining methodology can be applied to arbitrary design parameters to formulate an accurate design space.
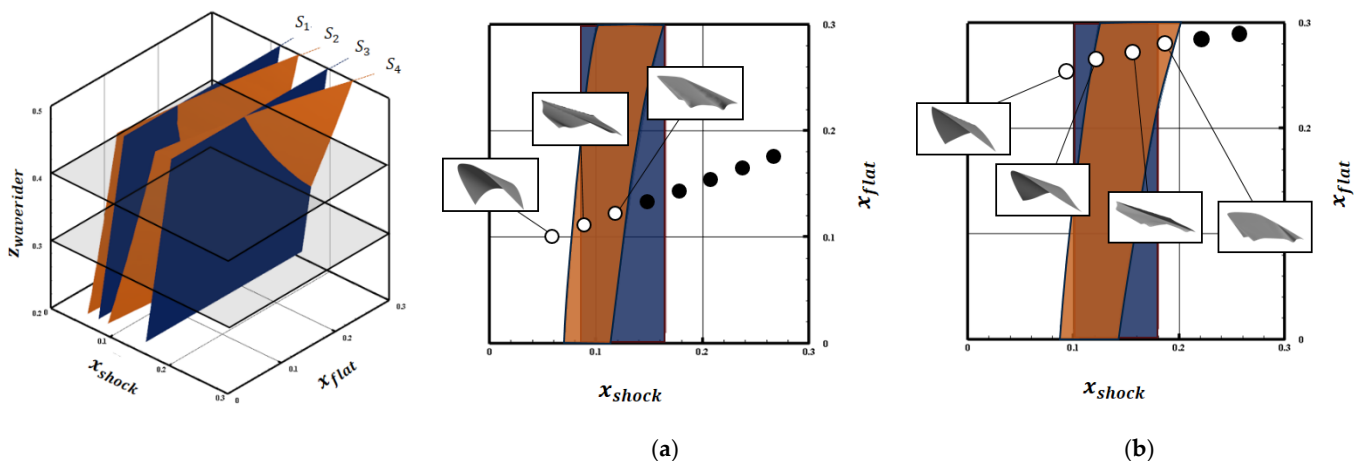

(a)

(b)

Figure 4. Design space comparison: (**a**) $z_{waverider} = 0.3$; (**b**) $z_{waverider} = 0.4$.

2.3. Performance Estimation Technique

As explained in Section 2.1, the DOE, CFD analysis, surrogate model construction and adaptive sampling techniques are required to represent the vehicle performance based on the configuration. This section describes each methodology used in this study.

The first step in constructing the model is selecting the initial sample points. Sample points should be selected such that they are evenly distributed in the design space. In this study, the initial sample points were selected using optimal Latin-hypercube sampling (OLHS), which enables uniform sampling for multivariate models [18].

KFLOW, a compressible solver based on a structured grid, was used to calculate the aerodynamic force acting on the waverider [19,20]. The Euler equation was applied to analyze the inviscid steady-state flow. The HLLE+ flux scheme [19] as the convective term and the Van Leer limiter of second-order accuracy were used for accurate and robust flow analysis. To ensure a steady-state calculation, the backward Euler method was applied with local time-stepping as a temporal integration scheme. The diagonalized alternating direction implicit method was used to calculate the inverse matrix. The Courant–Friedrichs–Lewy (CFL) number was set at 0.5.

Figure 5 shows a grid system used in this study. The grid independency analysis was conducted on this grid system The corresponding results were listed in Table 1. The lift coefficients are sufficiently accurate even in the coarse grid. However, the drag coefficient shows a considerable error between the coarse grid and the fine grid. In particular, since the drag coefficient will be used as the objective function of this study, 7,180,000 grids were used for the grid system.
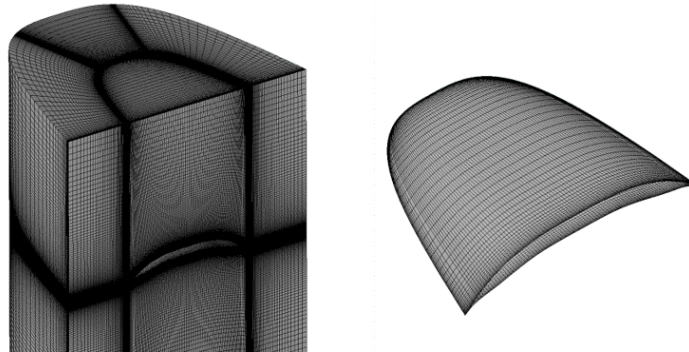

Figure 5. Grid system of the waverider.

Table 1. Grid independency analysis results.

Cases	Grid Size	C_L	C_D
Coarse 1	$1,709,960$	1.091	2.195×10^{-1}
Coarse 2	$3,578,542$	1.091	2.177×10^{-1}
Moderate	$7,180,000$	1.091	2.165×10^{-1}
Fine	$14,372,820$	1.091	2.151×10^{-1}

The CFD code used herein was validated against the experimental results of an all-body hypersonic aircraft [21]. The experimental conditions were as follows: $M_\infty = 7.4$, $Re_\infty = 15 \times 10^6$, $T_\infty = 62K$, $T_w = 300K$, and $\alpha = 0°$, $5°$, $10°$, and $15°$. Based on each angle of attack (AOA), the windward and leeward centerline surface pressures were obtained through experiments. Figure 6 illustrates the experimental and numerical results. Since the Euler solver was employed in this study, the viscous effect could not be included in the results. Therefore, CFD results were slightly underpredicted compared to the experiments owing to the boundary layer effect. However, the numerical results for two low AoA cases concurred well. This study is primarily focused on the waverider that cruises at an AOA of $0°$ with a slender body shape. In other words, the flow characteristics around the waverider correspond to the physical area when the AOA is low among the experimental results. Therefore, sufficiently accurate aerodynamic data can be obtained by applying the Euler solver used herein.

The aerodynamic performance is calculated for sample points selected through the OLHS with Euler solver. The surrogate model was generated using the performance data. In this study, we used a kriging model suitable for a deterministic computer model [22]. The kriging model is expressed as indicated in Equation (6) for the input variable vector x.

$$y(x) = \beta + Z(x), \tag{6}$$

where β denotes a global model, which is the trend of the entire domain, and $Z(x)$ represents a local deviation, correcting the kriging model value based on each sample point. A correlation function is defined as a function of distance to determine the global model and local deviation. The model parameter that best predicts the value of the sample points is determined through maximum likelihood estimation.
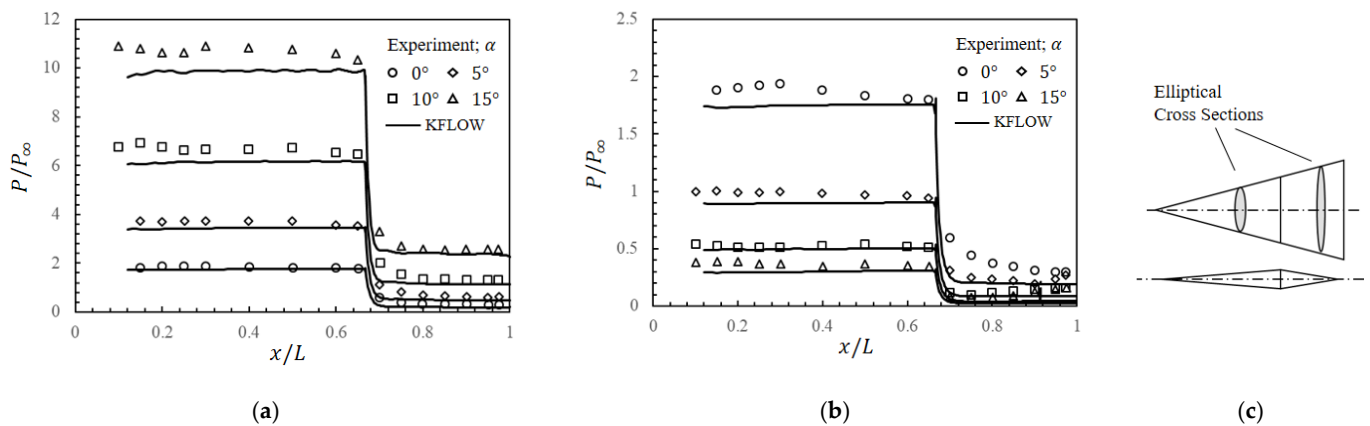
Figure 6. Effect of angle of attack on centerline surface pressures: (**a**) windward cases; (**b**) leeward cases; experimental model (**c**) all-body model [21].

The constructed model can be efficiently enhanced by adding certain data points. Expected improvement (EI) is a method of selecting sample points to be added to improve model accuracy [23]. The model accuracy can be effectively improved by adding a small number of sample points with EI. Equation (7) is used to select additional sample points in EI. The first term of Equation (7) increases when the distance between the design point and optimum point reduces. The second term exhibits a high value when the uncertainty of the model is large. The combination of these two values can generate the design point with a high model uncertainty around the optimum point. Thus, the accuracy of the model can be improved significantly by selecting this point as an additional sample point.

$$E[I] = (f_{min} - \hat{y})\Phi\left(\frac{f_{min} - \hat{y}}{s}\right) + s\phi\left(\frac{f_{min} - \hat{y}}{s}\right). \tag{7}$$

The surrogate model is modified by the performance estimation data of the added sample points. This process is repeated until the generated model attains a certain level of accuracy. Finally, optimization is performed using the completed model.

3. Results and Discussion

3.1. Progress of Direct Optimization

This section explains the application of the proposed direct design optimization method to the design problem. Section 3.1 presents the problem definition, which includes defining the objectives, constraints and design parameters. Section 3.2 describes the process of model construction to be used for optimization.

3.1.1. Problem Definition

The primary concern of hypersonic flight is the high wave drag and aerodynamic heating. Owing to aerodynamic heating, hypersonic vehicles require additional volume for internal components, such as the thermal protection system. Since the drag and internal volume of the vehicle are in a trade-off relationship, it is crucial to identify a concurrence between them. In this regard, two objectives, namely minimizing the drag coefficient and maximizing the internal volume of the waverider, were considered herein. The lift coefficient was selected as the constraint to support the mission payload. In the case of design conditions, the altitude was set at 25 km, Mach number at 5, and shockwave angle β at 15°. The other atmospheric quantities, such as temperature or density, were set based on the US standard atmosphere data [24]. The design problem can be summarized as follows: Bulleted lists look like this:

- Obj 1 Minimize C_D;
- Obj 2 Maximize Internal Volume;

- Subject to $C_L \geq C_{L,baseline}$;
- under : $M_\infty = 5$, $\beta = 15°$, altitude $= 25$ km.

Owing to the inverse design problem of the waverider, it is difficult to set a design parameter that achieves a balance between over-parameterizing and over-restricting. To address this problem, Kontogiannis investigated the DOF of various parameterization methods for waverider design curves based on the osculating cone theory [13]. Herein, we employed an efficient design parameterization method of Kontogiannis, which exhibits a high DOF of design while using a small number of design parameters. The right-hand side of the symmetry plane in Figure 3 depicts the design curves and design parameters of this study. The height is the largest vertical distance between the shockwave and the upper surface, and the width is the horizontal distance from the symmetry plane to the end of the span direction. The height was fixed at 1.34 m, which set the length and width of the vehicle at 5 m and 3 m, respectively. The shockwave curve comprises a straight line and a fourth-order Bezier curve. The horizontal length of the straight line was expressed as X1 normalized to the width. The Bezier curve used five control points, wherein four points were positioned parallel to the straight line to ensure second-order differential continuity required for the osculating cone theory. Additionally, the five control points were evenly positioned horizontally. Based on these two conditions, only one variable was used for the shockwave curve, namely the height of the rightmost control point, which is expressed as X2 normalized with height. The upper surface curve comprised only a fourth-order Bezier curve, and four control points were used to define the upper surface of the Bezier curve. All control points were evenly distributed in the horizontal direction. The positions of the leftmost and rightmost control points were determined by the height, width, and X2. Therefore, we used only two design variables that define the vertical position of the inner two control points. The vertical distances between the two points and the center of the upper surface are expressed as X3 and X4. Both these variables are normalized with $(1 - X2)$, which indicates the vertical distance between the rightmost control point and the center of the upper surface. Table 2 summarizes the design variables, wherein the range of each design variable is set to 0 to 1.

Table 2. Design variables.

Design Variable	Description
X1	Flat region of the shockwave curve normalized with the width
X2	Height of the shockwave curve normalized with the height
X3	Vertical distance from the upper surface normalized with the height $(1 - X2)$
X4	Vertical distance from the upper surface normalized with the height $(1 - X2)$

Figure 7 illustrates examples of waverider configurations viewed from the top and rear. The leading-edge shape viewed from the top and the upper surface shape viewed from the rear vary from sharp to curved and flat, respectively. The rearview indicates that the backside of the vehicle can demonstrate various design shapes. Therefore, various types of waverider shapes can be derived with only four design variables because the efficient parameter was employed in this study.
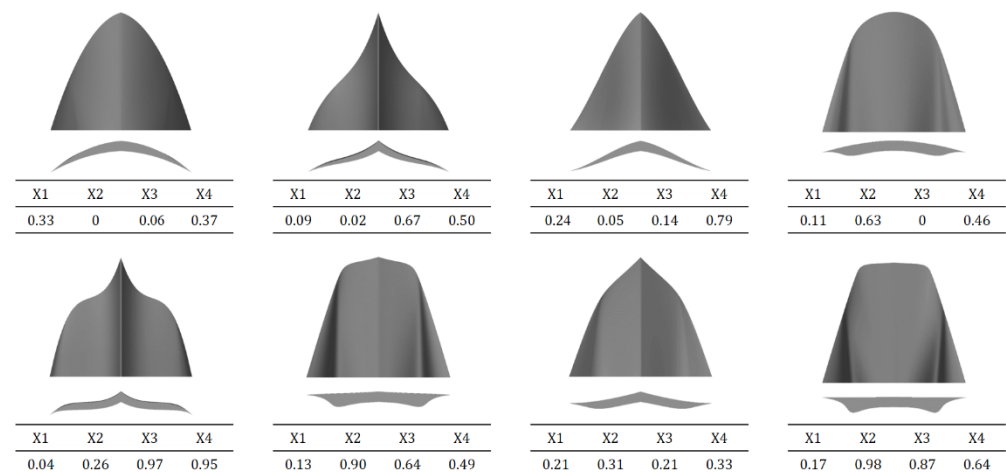
X1	X2	X3	X4
0.33	0	0.06	0.37

X1	X2	X3	X4
0.09	0.02	0.67	0.50

X1	X2	X3	X4
0.24	0.05	0.14	0.79

X1	X2	X3	X4
0.11	0.63	0	0.46

X1	X2	X3	X4
0.04	0.26	0.97	0.95

X1	X2	X3	X4
0.13	0.90	0.64	0.49

X1	X2	X3	X4
0.21	0.31	0.21	0.33

X1	X2	X3	X4
0.17	0.98	0.87	0.64

Figure 7. Examples of waverider configurations with various design parameters: $M_\infty = 5$, $\beta = 15\,°$, *width* = 3 m, and *height* = 1.34 m.

We formulated the design space by applying the design space-defining methodology presented in Section 2.2. Equation (8) presents the design space used in this study. The large value on the left-hand side of the equation implies that the distance between the upper surface and the center of the local osculating cone is short. The influence of X3 and X4 was ignored because the design space was defined based on the center of the upper surface. In the optimization process, 10% of the offset was applied to the right-hand side of Equation (8) to avoid the tolerance problem, which can occur owing to computing errors.

$$\frac{X2}{(1 - X1)^4} < \frac{7}{64}\left(\frac{width}{height}\right)^4. \tag{8}$$

The baseline waverider configuration was generated using the same design parameter with the median value of the design variable range. The range of each design variable is set between 0 and 1. The constraint of Equation (8) is violated if the values of the four design variables are set to 0.5. To prevent this, the value of the design variable X1 was set at 0.25, whereas the remaining values were set at 0.5.

3.1.2. Model Construction

Surrogate models were constructed considering the drag force, internal volume, and lift force to optimize the design. The drag and lift forces were estimated using the KFLOW based on the Euler equation. The internal volume was calculated using the generated waverider configuration. We developed an initial kriging model using 34 initial sample points generated based on the OLHS. Furthermore, EI was applied to the initial kriging model to improve its accuracy by adding the data points selected using Equation (7). Three sample points were added at each iteration, wherein two points maximize the EI values for each of the two objective functions used in this study. The other point maximizes the sum of the two EI values of each objective function. The process of sample point addition was repeated until the error for all three added points was within 3%. Figure 8 illustrates the error of the model for each objective function and its averaged value based on the refinement process. The drag coefficient error gradually decreased with the decrease in the number of EI refinement processes. Although the volume error did not decrease significantly and remained at a certain level, the average of the two values decreased to 3.24%. We performed nine iterations with three sample points added in each iteration. The final 60 sample points, excluding one point because of the grid generation problem, were used to construct the kriging model.
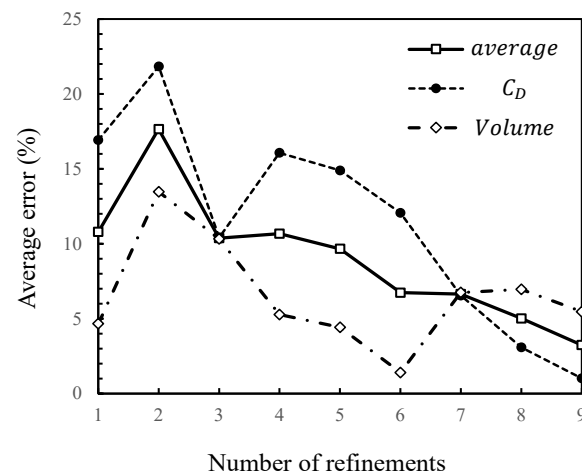
Figure 8. Model error with the refinement process.

We performed cross-validation of the constructed kriging model to calculate the goodness of fit between the model and the flow solver [23,25]. Figure 9 depicts the result of cross-validation with the entire sample points indicated in the figure. The horizontal axis represents the calculated value derived from the flow solver, whereas the vertical axis represents the value predicted by the kriging model. The model is considered accurate if sample points are closer to the diagonal line of symmetry.

| (a) | (b) | (c) |
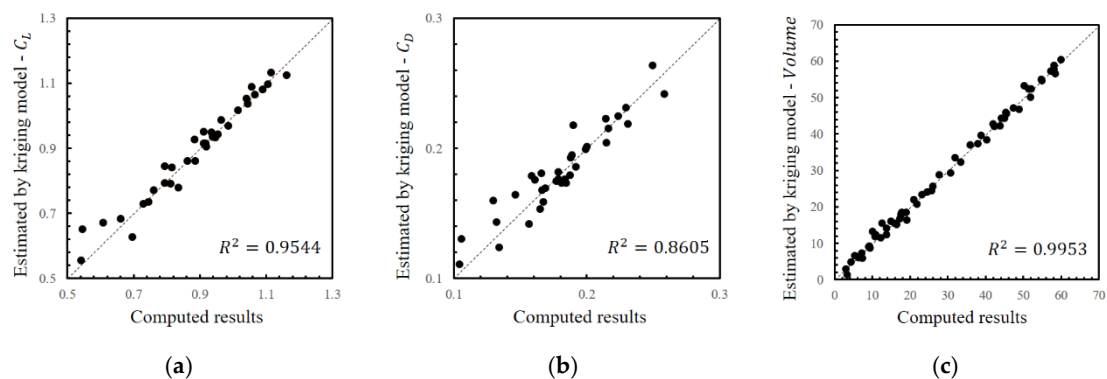
Figure 9. Cross-validation data required for the kriging model; (**a**) lift coefficient; (**b**) drag coefficient; (**c**) internal volume.

The EI method selects the sample points that are used to improve the accuracy of the model based on the value of the objective functions and constraints. Therefore, the accuracy of the model varies according to the predicted value of the model. For instance, the lift coefficient model with a value greater than 0.8 can be considered accurate, as illustrated in Figure 9a. This is because the additional sample points were selected to satisfy the constraint defined by a lower lift limit. Conversely, in the drag coefficient model, only the sample points around the 0.2 value are close to the diagonal line. This result can be attributed to two reasons. First, the EI process selects the sample points with a low drag value because the design objective is defined as drag minimization. These sample points improve the accuracy of the low-value region of the model. Second, the lower lift limit constraint prevents the additional sample points from exhibiting a low drag value because the lift and drag share a positive correlation.

As the additional sample points are selected to adhere to the optimization problem, the regions of the lift and drag model with high accuracy obtained through the EI process contain the solution of the optimal problem. Therefore, the optimization process can successfully determine the optimal solution with the constructed lift and drag models.

Furthermore, the volume model exhibited high accuracy over all areas, as plotted in Figure 9c. Therefore, the entire constructed model is sufficiently accurate to be used for optimization.

We investigated the effect of each design variable on the constructed surrogate model. We performed the ANOVA to identify the effect of the design variable by decomposing the variance of the model based on the design variables [26]. The results of the ANOVA that quantify the proportion of the influence of each design variable are plotted in Figure 10. As indicated in the figure, the design variable X2 is dominant in all three models. As X2 defines the height of the shockwave, it exhibits the most pronounced effect on the curvature of the shockwave among the four design variables. The curvature of the shockwave determines the location of the center of the cone on the osculating plane, which is a crucial factor in determining the basic flow field. Therefore, the flow properties around the vehicle are primarily affected by X2. Additionally, as variables X3 and X4 were normalized to X2, X2 significantly influences all models. In the case of the drag coefficient model, the effect of X3 is stronger compared to that of X4. This result indicates that the shape of the central area of the vehicle is associated with the drag coefficient. In contrast, X4 affects the volume model more than X3, which implies that the side area of the vehicle influences the volume.
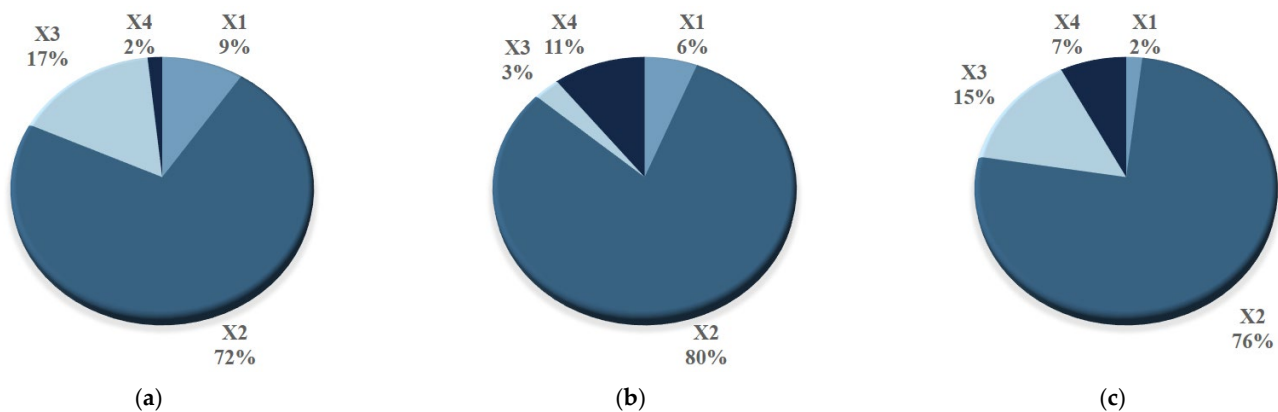

Figure 10. Analysis of variance (ANOVA) results for the constructed kriging model; (**a**) drag coefficient; (**b**) internal volume; (**c**) lift coefficient.

3.2. Design Optimization

In this section, optimal solutions obtained from the genetic algorithm are discussed in terms of objectives and constraints. Furthermore, flow characteristics around the waverider are analyzed by re-performing the flow analysis on the optimal solutions. Finally, the decision tree analysis is performed to identify the general characteristics of the waverider.

3.2.1. Optimized Results

Optimization was performed through a genetic algorithm using the constructed kriging model. The population size and generation size were 256 and 100, respectively. The crossover rate and mutation rate were fixed at 1 and 0.1. Through the optimization process, 111 non-dominated solutions were obtained. Figure 11 illustrates the relationship between the drag coefficient and a geometric constraint of each optimal solution. The geometric constraint is the value of the left-hand side in Equation (8), which determines whether the design point is included in the design space. The dashed line indicates the boundary of the design space, and the shaded area represents the region outside the design space. As plotted in Figure 11, the geometric constraint value increases with the increase in the drag coefficient and remains constant after encountering the boundary of the design space. Although optimal solutions after the boundary encounter exhibit a constant geometric constraint value, these solutions present a wide range of drag. This is because the values of design variables X3 and X4 can be different here, as these two design variables were not considered in Equation (8). The optimal solutions with a constant geometric constraint

exhibit a large internal volume, which is the second objective. Design points for these optimal solutions are close to the boundary of the design space. If the design space is not accurate, the boundary changes, and the design points that lie on the boundary can be lost. In this case, the optimization process cannot determine the optimal solutions. To prevent this situation, the design space must be accurately defined. Therefore, the proposed design space-defining methodology that can accurately derive the design space is necessary when designing an osculating cone theory-based waverider.
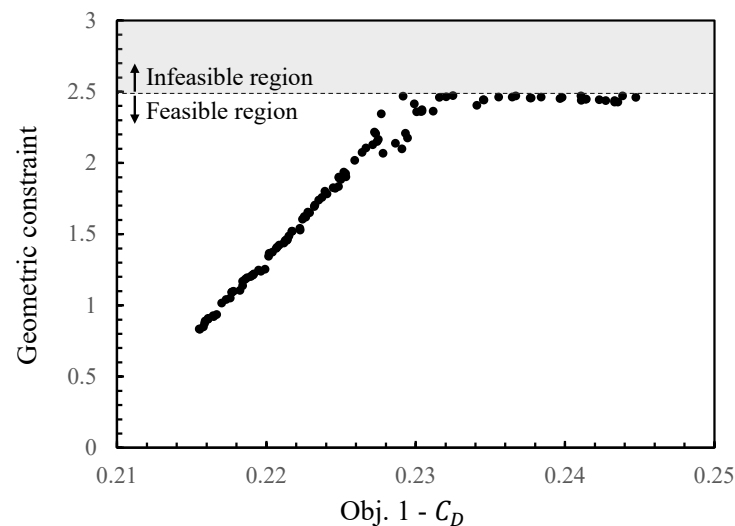
Figure 11. Drag coefficient and geometric constraint for optimal designs.

The Pareto front for the non-dominated solutions is shown in Figure 12. The horizontal and vertical axes are drag coefficient and internal volume, respectively. The areas with low performance compared to the baseline were shaded. Twelve representative solutions out of the 111 solutions were obtained by sorting the entire solutions in the order of the drag coefficient and selecting the solutions to have nine solution intervals. In order to identify the characteristics of the waverider configuration by classifying the 12 representative solutions, the K-mean clustering method, a famous data mining method, was used for this study [27]. As a result of K-mean clustering, 12 solutions were classified into four groups. The top and back view of each solution was plotted in Figure 12. The design variables and geometric constraint—defined by the left-hand side of Equation (8)—values of the 12 solutions are shown in Table 3.

Table 3. Design variables and geometric constraint for representative optimal solutions.

|		X1	X2	X3	X4	Constraint
	OPT 1	0.002	0.828	0.306	0.183	0.83
Group 1	OPT 2	0.051	0.824	0.351	0.198	1.02
	OPT 3	0.088	0.826	0.393	0.184	1.19
	OPT 4	0.119	0.826	0.418	0.194	1.37
	OPT 5	0.142	0.826	0.430	0.200	1.52
Group 2	OPT 6	0.166	0.825	0.442	0.202	1.70
	OPT 7	0.186	0.828	0.431	0.191	1.88
	OPT 8	0.217	0.829	0.419	0.186	2.21
Group 3	OPT 9	0.230	0.849	0.418	0.084	2.41
	OPT 10	0.225	0.881	0.317	0.020	2.44
Group 4	OPT 11	0.226	0.885	0.168	0.044	2.47
	OPT 12	0.226	0.882	0.034	0.001	2.46
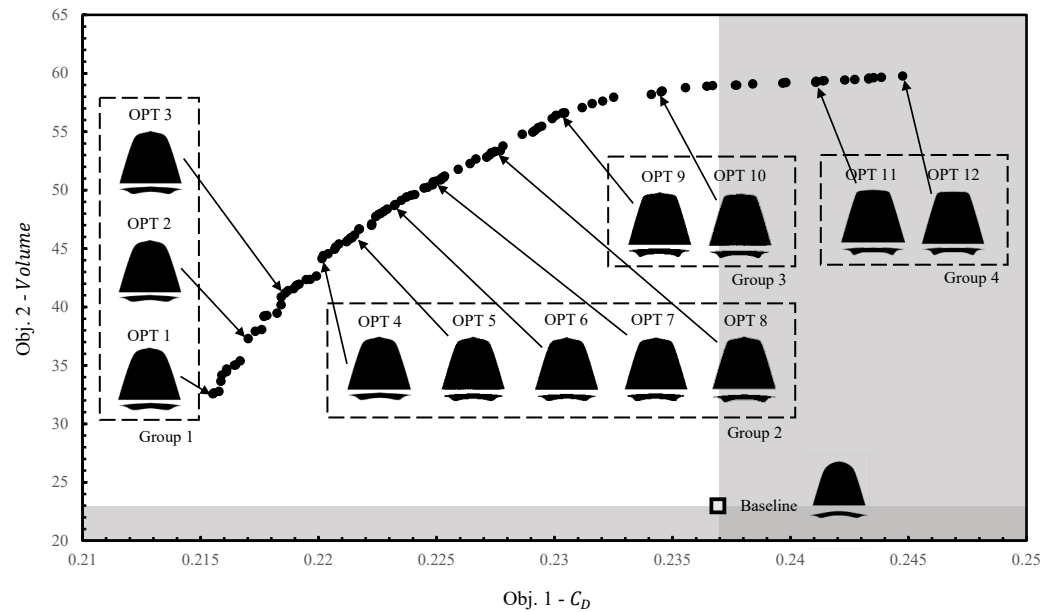
Figure 12. Optimal points and Pareto front estimated by kriging model.

As listed in Table 3, the value of X1 in solutions of group 1 is lower compared to those in the other groups. A low X1 value reduces the curvature of the shockwave attached to the waverider. Therefore, a geometric constraint value of group 1 is lower than those of the other groups because the distance between the center of the local osculating cone and the shockwave on the osculating plane is large. The X1 value in group 2 gradually increases from OPT 4 to OPT 8, which in turn increases the geometric constraint values for group 2. Finally, the geometric constraint value is maximized at group 3 and group 4 due to high X1 and X2 values.

Geometric constraint values for groups 3 and 4 are maximized owing to the high X1 and X2 values. The X3 and X4 values of group 4 are the lowest among all groups. As the X3 and X4 are decreased, the upper surface of the waverider is formed higher. The higher upper surface configuration causes the center of the local osculating cone to approach the upper surface.

Figure 13 shows the lateral cross-sections of OPT1 and OPT12. In sections (a) and (d), the curvature of the lower surface of the two configurations is similar. However, the lower surface of OPT12 partially protrudes at section (b) and protrudes very large in section (c). This is the effect of a high geometric constraint value, given in groups 3 and 4. A high geometric constraint value implies that the distance between the center of the osculating cone and the shockwave is short. Hence, the initial point of the streamline tracing, which is the leading-edge point, is close to the center of the cone. When the initial point of the streamline approaches the center of the cone, the angle between the streamline and the centerline of the cone increases considerably. Consequently, the lower surface of the waverider defined by the streamline approaches the shockwave. Owing to this process, both ends of the waverider configuration of groups 3 and 4 protrude, which expands the volume of the waverider. To conclude, a high curvature of the shockwave increases the internal volume.
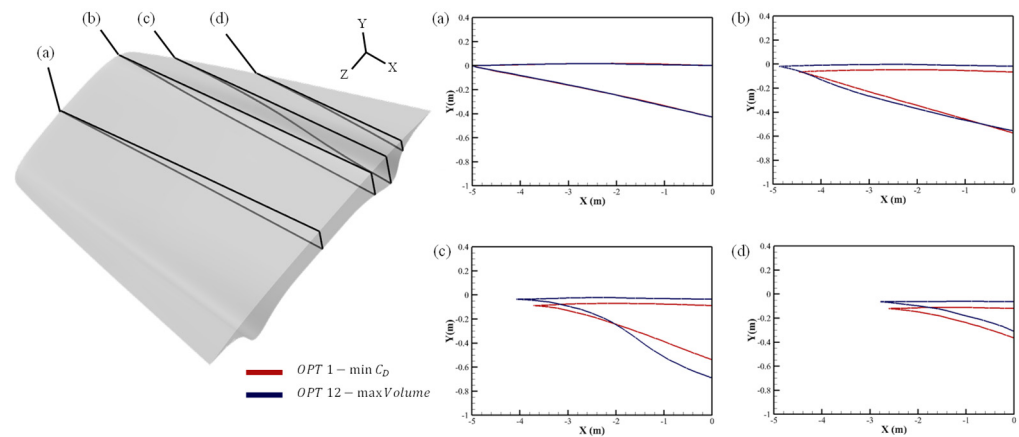
Figure 13. Lateral cross-sections diagram of OPT 1 and OPT 12; (**a**) $z = 0$ m; (**b**) $z = -1.4$ m; (**c**) $z = -1.8$ m; (**d**) $z = -2.2$ m.

The upper surface shape is formed upwards due to the low X3 and X4 of OPT 12, and the leading edge moves forward. As a result, the length of OPT 12 is longer than that of OPT 1, as shown in Figure 13b–d. At the same time, the higher upper surface also decreases the distance between the local osculating cone vertex and the upper surface. Therefore, low X3 and X4 values induce a large internal volume.

The performance analysis was repeated for the baseline shape, OPT 1, and OPT 12 to calculate the objective values accurately and identify the detailed characteristics of the flow field. Figure 14 depicts the flow analysis results for the baseline, OPT 1, and OPT 12. According to the characteristics of the waverider, the shockwave is attached to the leading edge of the vehicle in all three cases. In the case of OPT 1, the drag coefficient decreased by 3.0%, and the volume increased by 51.5% from the baseline. In OPT 12, which maximized the internal volume, the volume increased by 159.9%. Although the drag coefficient increased by 5.65% in comparison with that of the baseline, the increase in performance was drastic.
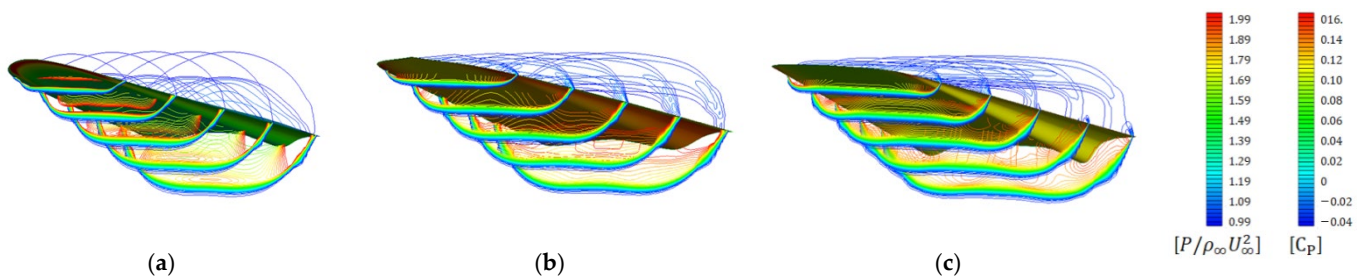

Figure 14. Computational fluid dynamics (CFD) results for optimal points and baseline configuration ($M_\infty = 5$, *altitude* = 25 km); (**a**) baseline; (**b**) optimum 1-minimal drag; (**c**) optimum 12-maximal volume.

Figure 15 illustrates the distribution of the pressure coefficient at the lower surface for OPT 1 and OPT 12. The pressure values around the plane of symmetry in the two cases are identical. However, the pressure at both ends of the vehicle is higher at OPT 12, and the pressure acting on the area between the ends and the plane of symmetry is higher at OPT 1. The shaded area is where the pressure of OPT 12 is higher than the pressure of OPT 1, and the striped area is the opposite. As optimized waveriders have a shape in which both ends protrude, the front projected area, which significantly affects the drag value, is large at both ends. Therefore, the shading area and the striped area are similar, but the drag is very different. In summary, the waverider has a lower drag when the protruding region is small. This is opposite to the shape of the waverider required for volume increase, and

it can be seen that the waverider has an inherent trade-off relationship between internal volume and drag.
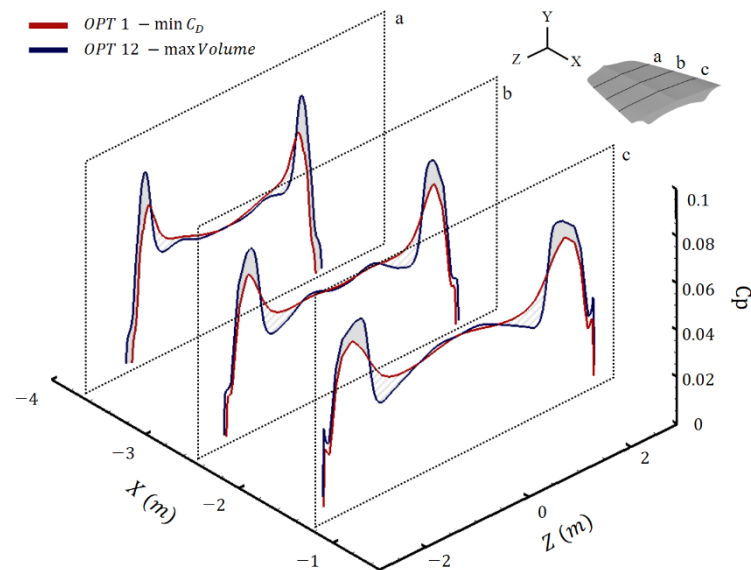

Figure 15. Lower surface pressure coefficient distribution for OPT 1 and OPT 12.

3.2.2. Decision Tree Analysis

In this study, we analyzed the design points using the decision tree analysis, which evaluates specific problems through statistical analysis of multivariate data [28]. The proposed design space-defining methodology facilitates this analysis because it corresponds to an exploration of the design space. The application of this method aids in identifying a set of design variables and a design rule that maximize or minimize the objective function. The decision tree analysis repeatedly divides the data into two subgroups to obtain results. The criteria for the classification of the two groups are determined by a specific design reference value. After several repetitions, a resultant subgroup that represents the design rule can be obtained.

Figure 16 illustrates the results of the decision tree analysis based on each objective function and the results of 60 CFD analyses. In the figure, r_{av} denotes the ratio of the mean of the current group objective function to the mean of the population objective function, and n indicates the number of data points in the group. Furthermore, the criteria used to classify the group are indicated in each box. The classification was conducted until the number of data points in the subgroup reached 10% of those in the population. The first design rule expressed for the volume is calculated using Equation (9).

$$if \ (X2 > 0.4338) \ and \ (X4 \leq 0.4834), \ then \ (r_{av} = 1.5329). \tag{9}$$

Identical to the ANOVA result, variables X2 and X4 classified the data with the highest accuracy. Limiting these two variables can facilitate the derivation of design results that increase the volume significantly. According to the expressed design rule, the values of X2 and X4 should be higher and lower than 0.4338 and 0.4834, respectively. As discussed above, when the value of X2 increases, the curvature of the shockwave and volume increase. When the value of X4 decreases, the distance between the center of the osculating cone and the upper surface decreases, which in turn increases the volume. OPT 1 and OPT 12 of this study strictly follow this design rule.

$$if \ (X2 \leq 0.1147) \ and \ (X1 \leq 0.5) \ and \ (X4 > 0.4358), \ then \ (r_{av} = 0.7445) \tag{10}$$
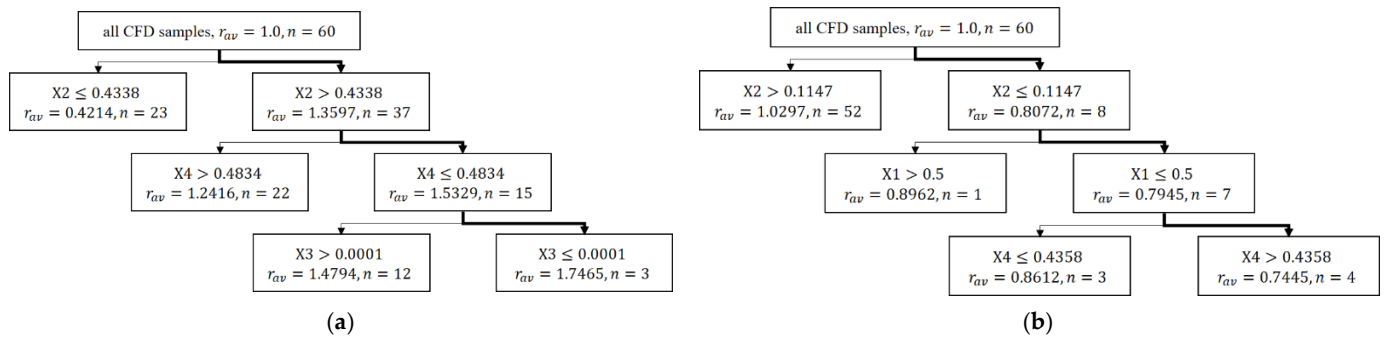
Figure 16. Decision tree analysis: (**a**) Geometric constraint based on the position of the cone center; (**b**) Geometric constraint based on the intersected planes.

Equation (10) represents the design rule for minimizing drag. The design variable X2 was selected as the first criterion. Unlike the first design rule (Equation (9)), design variables X2 and X1 should be low, and X4 should be high to exhibit a low drag. These values correspond to the large distance between the center of the osculating cone and the upper surface of the waverider. Therefore, the results of the two design rules indicate that the internal volume and drag of the waverider rely on the location of the center of the cone and upper surface. Unlike the optimization results which have lift coefficient constraints, decision tree analysis was applied for the entire design space. To conclude, the above results can be regarded as a general characteristic of waverider.

4. Conclusions

To address the inherent issues in the inverse waverider design, a novel direct design method for a waverider is proposed. We performed multi-objective design optimization for the drag and internal volume. The conclusions of the analysis of the proposed design method and design results can be summarized as follows:

(1) We developed a general approach to define the design space, which can be applied to an arbitrary set of design parameters of a waverider using the osculating cone theory. To this end, the failure conditions of the waverider inverse design used in the literature were classified into two geometric relationships, which were mathematically analyzed and determined to be redundant. Based on the analysis, we obtained a discriminant formula that unifies the two conditions. The design space for the waverider can be derived by applying the discriminant formula to the design curves. We observed that the obtained design space was more accurately represented than the reference model based on the ad hoc relation;

(2) Further, general characteristics of the waverider were derived using data mining methods, such as K-means clustering and decision tree analysis. The aerodynamic performance and the shape of the waverider were primarily affected by the curvature of the shockwave. The large curvature of the shockwave reduced the distance between the cone vertex of the osculating plane and the upper surface point. Consequently, the lower surface tends to approach the shockwave. As a result, the ends of the waverider protrude, and the internal volume increases. This protruding region increases the drag acting on the waverider. In summary, the waverider has an inherent geometric trade-off relationship between internal volume and drag;

(3) In the proposed design framework, the aerodynamic performance of the aircraft was directly considered an objective or constraint during the design process, which is one of the primary strengths of the direct design method. The computational efficiency required for the direct design method was achieved using surrogate models derived from high-fidelity flow analyses.

Appendix A. Osculating Cone Theory

The osculating cone theory is used to generate the basic flow field, which is the initial step in the waverider inverse design. The flow is approximated using a spanwise combination of the conical flow field. To generate the basic flow field, the desired 2D shockwave shape is initially defined on the base plane, as depicted in Figure A1 The shockwave is then discretized into a set of shockwave points. The plane that passes through the shockwave point and is perpendicular to the shockwave and the base plane is identified as the osculating plane. If the radius of curvature is calculated at each point of the shockwave, and the center of the cone is located at a certain distance based on the size of the radius of curvature within the osculating plane, the flow of the cone and the flow generated by the shockwave defined in the base plane can be considered similar. If the change in curvature of the shockwave is not large and the conical flow of each osculating plane is derived from the same shockwave angle, the shockwave of each osculating plane exhibits similar strength. In this case, the flow independence between the osculating planes is ensured, as the spanwise gradient is not large. The actual flow field can be approximated by combining the flows on the osculating planes.
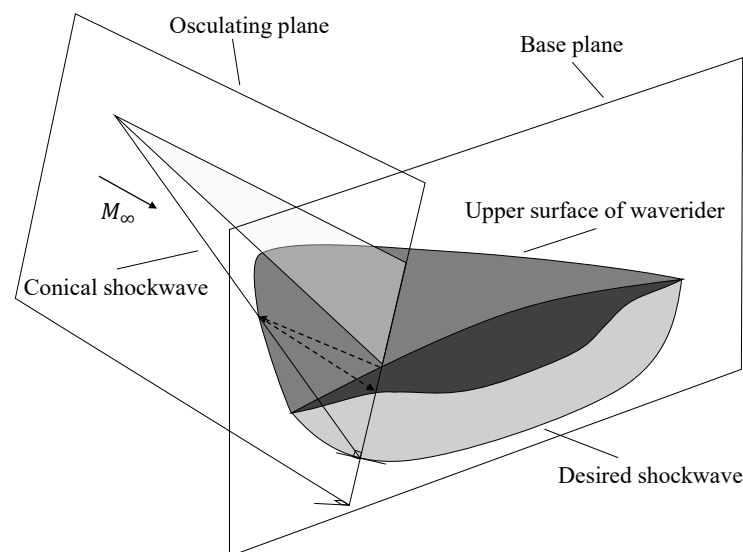

Figure A1. Osculating cone theory based waverider.

Subsequently, the process of waverider shape derivation is performed on each osculating plane. Herein, the upper surface on the base plane is defined to derive the waverider shape. After identifying the intersection point with the upper surface in each osculating

plane, the point in the upstream direction of free flow is moved, and the intersection point with the shockwave generated by the cone can be determined. This intersection is considered the leading edge of the waverider shape, and the path created by the movement of the point serves as the upper surface of the waverider. This is followed by tracing the streamline of the osculating plane flow at each leading edge, and the generated streamline is used as the bottom surface of the waverider. As the streamline and the wall surface must be parallel according to the boundary conditions of the flow after the shockwave, the wall surface generated by this streamline and the cone of the osculating plane must produce identical shockwaves. Accordingly, when the upper and bottom lines of all osculating planes are combined, a shockwave is attached along the leading edge of the vehicle. In this process of deriving the waverider shape, the flow analysis is performed only for the conical flow of a single shockwave angle, which considerably reduces the time required for the design in comparison with other methods. However, the osculating cone theory can be effectively applied to the design because it can generate sufficiently diverse basic flow field shapes.

References

1. Jackson, K.; Gruber, M.; Barhorst, T. The HIFIRE flight 2 experiment: An overview and status update. In Proceedings of the 45th AIAA/ASME/SAE/ASEE Joint Propulsion Conference & Exhibit, Denver, CO, USA, 2–5 August 2009. [CrossRef]
2. Küchemann, D. Hypersonic aircraft and their aerodynamic problems. *Prog. Aerosp. Sci* **1965**, *6*, 271–353. [CrossRef]
3. Nonweiler, T.R. Aerodynamic problems of Manned Space Vehicles. *RAeS* **1959**, *63*, 521–528. [CrossRef]
4. Ding, F.; Liu, J.; Shen, C.-b.; Liu, Z.; Chen, S.-h.; Fu, X. An overview of research on Waverider Design methodology. *Acta Astronaut.* **2017**, *140*, 190–205. [CrossRef]
5. Jones, J.G.; Moore, K.C.; Pike, J.; Roe, P.L. A method for designing lifting configurations for high supersonic speeds, using axisymmetric flow fields. *Ing. Arch.* **1968**, *37*, 56–72. [CrossRef]
6. Rasmussen, M.L. Waverider Configurations Derived from Inclined Circular and Elliptic Cones. *J. Spacecr. Rocket.* **1980**, *17*, 537–545. [CrossRef]
7. Sobieczky, H.; Dougherty, F.C.; Jones, K.D. Hypersonic Waverider Design from Given Shock Waves. In Proceedings of the First International Hypersonic Waverider Symposium, College Park, MD, USA, 17–19 October 1990.
8. Chen, L.; Guo, Z.; Deng, X.; Hou, Z.; Wang, W. Waverider configuration design with variable shock angle. *IEEE Access* **2019**, *7*, 42081–42093. [CrossRef]
9. Zheng, X.; Li, Y.; Zhu, C.; You, Y. Multiple osculating cones' waverider design method for ruled shock surfaces. *AIAA J.* **2019**, *58*, 854–866. [CrossRef]
10. Liebeck, R.H. Subsonic airfoil design. In *Applied Computational Aerodynamics*; Henne, P.A., Ed.; Progress in Astronautics and Aeronautics: New York, NY, USA, 1990; Volume 125, pp. 133–165. [CrossRef]
11. Labrujere, T.E.; Slooff, J.W. Computational methods for the aerodynamic design of aircraft components. *Annu. Rev. Fluid Mech.* **1993**, *25*, 183–214. [CrossRef]
12. Takashima, N. Optimization of Waverider—Based Hypersonic Vehicle Designs. Ph.D. Thesis, University of Maryland, College Park, MD, USA, 1997.
13. Kontogiannis, K.; Sóbester, A.; Taylor, N. Efficient Parameterization of Waverider Geometries. *J. Aircr.* **2017**, *54*, 890–901. [CrossRef]
14. Lobbia, M.A. Multidisciplinary Design Optimization of Waverider-Derived Crew Reentry Vehicles. *J. Spacecr. Rocket.* **2017**, *54*, 233–245. [CrossRef]
15. Lobbia, M.A. Rapid Supersonic/Hypersonic Aerodynamics Analysis Model for arbitrary geometries. *J. Spacecr. Rocket.* **2017**, *54*, 315–322. [CrossRef]
16. Goldberg, D.E. *Genetic Algorithms in Search, Optimization and Machine Learning*; Addison-Wesley Longman Publishing Co., Inc.: Boston, MA, USA, 1989.
17. Fonseca, C.M.; Fleming, P.J. Genetic Algorithms for Multiobjective Optimization: FormulationDiscussion and Generalization. *ICGA* **1993**, *93*, 416–423. [CrossRef]
18. Park, J.-S. Optimal latin-hypercube designs for computer experiments. *J. Stat. Plan. Inference* **1994**, *39*, 95–111. [CrossRef]
19. Park, S.H.; Lee, J.E.; Kwon, J.H. Preconditioned Hlle method for flows at all Mach numbers. *AIAA J.* **2006**, *44*, 2645–2653. [CrossRef]
20. Hong, Y.; Lee, D.; Yee, K.; Park, S.H. Enhanced high-order scheme for high-resolution rotorcraft flowfield analysis. *AIAA J.* **2022**, *60*, 144–159. [CrossRef]
21. Lockman, W.K.; Lawrence, S.L.; Cleary, J.W. Flow over an all-body hypersonic aircraft—Experiment and Computation. *J. Spacecr. Rocket.* **1992**, *29*, 7–15. [CrossRef]
22. Martin, J.D.; Simpson, T.W. Use of Kriging models to approximate deterministic computer models. *AIAA J* **2005**, *43*, 853–863. [CrossRef]

23. Jones, D.R.; Schonlau, M.; Welch, W.J. Efficient Global Optimization of Expensive Black-Box Functions. *J. Glob. Optim.* **1998**, *13*, 455–492. [CrossRef]

24. Pasquale, M.S. *Commercial Airplane Design Principles*, 1st ed.; Elsevier: Amsterdam, The Netherlands, 2014; pp. 487–495. [CrossRef]

25. Lee, S.; Yee, K.; Rhee, D.-H. Optimization of the array of film-cooling holes on a high-pressure turbine nozzle. *J. Propuls. Power* **2017**, *33*, 234–247. [CrossRef]

26. Jeong, S.; Chiba, K.; Obayashi, S. Data mining for aerodynamic design space. *J. Aeros. Compt. Inf. Commun* **2005**, *2*, 452–469. [CrossRef]

27. Lloyd, S. Least squares quantization in PCM. *IEEE Trans. Inf. Theory* **1982**, *28*, 129–137. [CrossRef]

28. Sugimura, K.; Obayashi, S.; Jeong, S. Multi-objective optimization and design rule mining for an aerodynamically efficient and stable centrifugal impeller with a vaned diffuser. *Eng. Optim.* **2010**, *42*, 271–293. [CrossRef]